Electron solvation in aqueous reverse micelles: Equilibrium properties

Daniel Laria
Unidad Actividad Química, Comisión Nacional de Energía Atómica, Avenida Libertador 8250 and Departamento de Química Inorgánica, Analítica y Química-Física e INQUIMAE, Facultad de Ciencias Exactas y Naturales, Universidad de Buenos Aires, Ciudad Universitaria, Pabellón II, 1428 Buenos Aires, Argentina

Raymond Kapral[a)]
Department of Chemistry, Chemical Physics Theory Group, University of Toronto, Toronto, Ontario M5S 3H6, Canada

(Received 12 February 2002; accepted 2 August 2002)

Microscopic aspects of electron solvation in aqueous reverse micelles are investigated using molecular dynamics simulation techniques. Two micelle sizes, with water/surfactant ratios of 3 and 7.5, are examined. The electron is treated quantum mechanically using Feynman path integral methods while the water, surfactant head groups, and counter ions are treated classically. Through computations of the free energy as a function of the radial distance, the electron is found to be preferentially solvated in the interior of the micelle in the ''bulk'' water pool. For small micelles, the presence of the electron leads to a depletion of water in the central region of the micelle and thus strongly disrupts the water equilibrium structure. Contact and solvent-separated ion pairs between the electron and Na^+ counter ions are found to play an important role in the equilibrium structure. For the two micelle sizes investigated, the most stable solvation structures correspond to contact ion pairs. The localization of the electronic charge distribution is found to increase with micelle size, signaling more efficient solvation in larger micelles.
[DOI: 10.1063/1.1509449]

I. INTRODUCTION

Reverse micelles are formed when surfactants are dissolved in neat organic solvents or in organic phases containing small amounts of water. In the latter case the reverse micelles comprise roughly spherical pools of water surrounded by the polar head groups of the surfactant molecules. Micelles with different sizes and properties can be made by changing the water/surfactant ratio in the solution. Reverse micelles of this type have been studied widely, primarily because of their usefulness as microreactors for chemical and biochemical reactions.[1,2] Not only can one carry out chemical reactions in a confined environment where the encounter rates between species are rapid compared to those in bulk phases but, since polar and nonpolar environments are brought into close proximity, one may efficiently carry out reactions that are difficult to achieve in bulk homogeneous environments.

Many of the unusual properties of reverse micelles stem from the peculiar nature of the water phase within the micelle. It is widely believed that the water phase may be partitioned into zones corresponding to ''surface'' water that is tightly bound to the surfactant head groups and associated counter ions, and ''bulk'' water at the center of micelle. The size of the reverse micelle and thus the relative amounts of these two water phases can be tuned by changing the ratio w_0=[water]/[surfactant]. Often the water structure within micelles is studied through its interactions with probe species. Solvated electrons produced by radiolysis or other means have provided considerable insight into the nature of the reverse micellar water structure.[3–7] In addition, many of the important chemical and biochemical reactions studied in reverse micelles involve electron transfer processes. In this context it is important to understand on a microscopic level how electron solvation takes place in the micellar environment.

Molecular-level studies of electron solvation in reverse micelles present a number of difficulties. The reverse micellar structure is complex, involving the formation of the micelle by arrangement of the surfactant head groups around the water pool and the stabilization of this structure. The configurational degrees of freedom of the tail groups play a central role in this stabilization process. There have been microscopic studies of micelles in which the full structure of the surfactant molecules has been taken into account.[8] One of the most thorough molecular-level studies of the reverse micellar structure was carried out by Faeder and Ladanyi[9] who used a simple model for the surfactant molecules. The tail groups were neglected by supposing that the interior of the micelle was confined by a spherical potential. The surfactant head groups extended into the water pool and were free to move on the micellar surface. The model captures many important features of real micelles so that one may investigate microscopic aspects of the structure in the water pool, but it is sufficiently simple that extensive studies of the structure and dynamics can be carried out for a range of micelle sizes.

[a)]Author to whom correspondence should be addressed. Electronic mail: rkapral@gatto.chem.utoronto.ca

If one wishes to study electron solvation in reverse micelles one must take into account the fact that the electron is a quantum object and cannot be treated classically. A full molecular description at a reasonable level of approximation must therefore consider a quantum electron in a classical environment comprising the surfactant molecules, counter ions, and water molecules. Simulations of electron structure in classical bulk environments have been carried out[10–13] by using a Feynman path integral representation of the electron.[14] The calculations are technically challenging because of the large number of effective polymer beads that are needed to simulate the discretized path integral. Special sampling methods have been devised to overcome these difficulties.[15–17]

In this paper we present a microscopic study of electron solvation in reverse micelles. We adopt the micellar model of Faeder and Ladanyi[9] and treat the electron by using discretized path integral techniques. Section II presents the details of the model and how it was simulated. In particular, the intermolecular potentials used to model the interactions are specified and the parameters needed to carry out the molecular dynamics simulations are given. The aim of the paper is to provide a detailed description of the solvation structure of the electron in the reverse micellar water pool. These results are presented in Sec. III. The conclusions of the study are given in Sec. IV.

II. MODEL

The equilibrium statistical mechanical description of the system may be cast in terms of Feynman's path integral formulation of quantum mechanics.[14] Quantum fluctuations are neglected for all particles, with the exception of the electron. In this formulation, the canonical partition function Q takes the form

$$Q \propto \int d\{\mathbf{R}\} e^{-\beta V_{\mathrm{cl}}(\{\mathbf{R}\})} \int \cdots \int \mathcal{D}[\mathbf{r}(t)] e^{-S[\mathbf{r}(t),\{\mathbf{R}\}]}, \quad (1)$$

where β^{-1} is the Boltzmann constant times the temperature, $V_{\mathrm{cl}}(\{\mathbf{R}\})$ denotes the potential energy for the classical particles with coordinates $\{\mathbf{R}\}$; $\mathbf{r}(t)$ represents the electron position at the imaginary time t and $\mathcal{D}[\mathbf{r}(t)]$ symbolizes the path integral. The action functional $S[\mathbf{r}(t),\{\mathbf{R}\}]$ is given by

$$S[\mathbf{r}(t),\{\mathbf{R}\}] = \frac{1}{\beta\hbar} \int_0^{\beta\hbar} dt \left(\frac{1}{2} m_e \dot{\mathbf{r}}^2(t) + V_{\mathrm{es}}(\mathbf{r}(t),\{\mathbf{R}\}) \right), \quad (2)$$

where m_e is the electron mass, $V_{\mathrm{es}}(\mathbf{r}(t),\{\mathbf{R}\})$ is the potential between the electron and the classical particles, and $2\pi\hbar$ is Planck's constant.

Before one can consider the simulation of the excess electron in a reverse aqueous micelle, one needs a reasonable model for the micelle in the absence of the electron; i.e., the water micropool surrounded by surfactants and a nonpolar phase. Since the experimental evidence suggests that the excess electrons reside mainly in the aqueous pools,[3–7] we focus our attention on electron solvation within these pools. Consequently, it is appropriate to use the simplified model of Faeder and Ladanyi[9] for the micelle where the effects of the hydrophobic portions of the amphiphiles and the nonpolar phase are taken into account through a confining potential that gives the micelle a spherical-like structure with radius R. This model is constructed to represent micelles formed using the sodium bis(2-ethylhexyl)sulfosuccinate (AOT) surfactant in dilute mixtures of water in nonpolar solvents. The SO_3^- head groups and Na^+ counter ions of the surfactant molecules are taken into account explicitly, an important feature for our microscopic solvation studies. Given these considerations, our model system includes: N_w water molecules, $N_{SO_3^-}$ surfactant head groups harmonically bound to a cavity of radius R, N_{Na^+} counter ions, and the excess electron.

The coupling of the electron to the other molecules in the micelle is described by the potential V_{es} which has three main contributions:

$$V_{\mathrm{es}} = V_{e-w} + V_{e-SO_3^-} + V_{e-Na^+}. \quad (3)$$

Here V_{e-w} is the electron–water potential which was taken from the pseudopotential model of Schnitker and Rossky.[11] Assuming a united atom model for the SO_3^- group, the electron–SO_3^- interaction $V_{e-SO_3^-}$ was taken to consist solely of pairwise additive Coulombic terms. For the electron–counter ion contribution V_{e-Na^+}, we adopted the local pseudopotential form given in Bachelet *et al.*[18] The contributions to the potential energy among the classical particles V_{cl} were taken to be identical to those in Faeder and Ladanyi,[9] except for the water–water interactions. To be consistent with the V_{e-w} of Schnitker and Rossky,[11] we used the SPC model[19] for water instead of the extended simple point charge (SPCE) model.[20] Simulations of electron solvation were carried out on micelles whose sizes were characterized by the ratios $w_0 = 3$ ($R = 13.2$ Å) and 7.5 ($R = 19.4$ Å); in addition some simulations were also carried out for larger micelles with $w_0 = 10$ ($R = 22.9$ Å). The geometrical parameters, and number of water and surfactant molecules were identical to those presented in Table II of Faeder and Ladanyi.[9]

A. Simulation method

Efficient algorithms exist to properly sample fluctuations of the electron path governed by the action in Eq. (2). These algorithms rely on the isomorphism that exists between the statistical mechanics of the electron path, discretized in imaginary time, and that of a cyclic polymer with P "beads" with coordinates $\mathbf{r}_i$.

For a finite value of P, the quantum partition function in Eq. (1) reduces to that of a classical system with an effective potential given by[21]

$$V_{\mathrm{eff}} = V_{\mathrm{cl}} + \frac{P m_e}{2(\beta\hbar)^2} \sum_{i=1}^{P} (\mathbf{r}_i - \mathbf{r}_{i+1})^2 + \frac{1}{P} \sum_{i=1}^{P} V_{\mathrm{es}}(\{\mathbf{r}_i\},\{\mathbf{R}\}). \quad (4)$$

To sample the phase space of a system governed by this effective potential, we implemented a molecular dynamics scheme that included a reversible multiple time scale integrator for Newton's equations of motion,[22] and the staging algorithm.[16] Full details of the method can be found in Refs. 15–17. The parameters employed in our simulations were as follows: the number of beads was taken to be $P = 1000$ and

the number of staging masses was set to $j-1=49$. The masses of the electron beads were taken to be equal to the actual mass of the electron $m_e^*=m_e$, while for the rest of the classical atomic species, the masses were taken to be $m_\alpha^*=10^{-2}m_\alpha$.

A chain of Nosé–Hoover thermostats[23] was used to simulate canonical dynamics. Chains consisting of three Nosé–Hoover thermostats set at $T=298\,\mathrm{K}$ were coupled to each Cartesian coordinate of the polymer–electron; an additional chain was also attached to the rest of the classical particles. The masses of these thermostat chains were set equal to $Q_e^{\mathrm{stage}}=\beta\hbar^2/P$ and $Q_e^{\mathrm{end}}=jQ_e^{\mathrm{stage}}$ for the stage and end beads, respectively. The masses of the chain of thermostats coupled to the classical particles were taken as $Q_1=N_d/(\beta\omega_{\mathrm{LJ}})$ and $Q_i=Q_1/N_d$ $(i=2,3)$, where N_d is the number of degrees of freedom in the classical system and ω_{LJ} is the frequency at the minimum of the oxygen–oxygen Lennard-Jones interaction in water. Constraints imposed on the intramolecular distances and on the particle positions were handled with the SHAKE algorithm.[24]

Two different time steps were used: $\Delta t=10^{-2}$ fs to integrate the classical bath variables and $\delta t=\Delta t/3$ to evolve the rest of the fast dynamical variables (including the thermostats). All simulations included an equilibration period of approximately $10^5\Delta t$, followed by trajectories of typical length $1-1.5\times10^6\,\Delta t$ used to evaluate the statistical properties of the system. Given the fictitious nature of the dynamics and the arbitrary assignment of light masses to the classical particles to better sample the phase space, no physical significance should be attached to the time intervals in the simulations. Rather, their length is proportional to the number of independent equilibrium configurations sampled in the simulation.

As we shall see in the results presented below, the equilibrium structure of electron solvation in reverse micelles is complicated by the existence of metastable ion pair species separated by high free energy barriers. As a result, straightforward molecular dynamics or Monte Carlo cannot be used to investigate the equilibrium structure and methods for rare event sampling must be implemented to study the nature of the metastable states in the system.

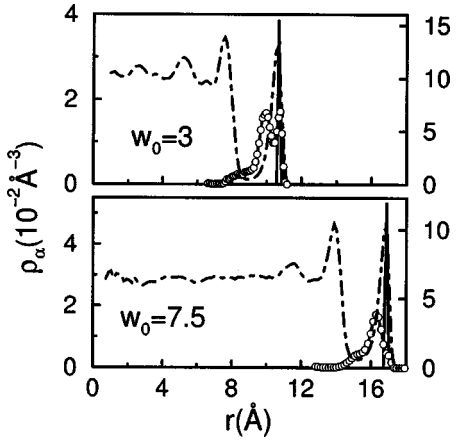

FIG. 1. Species density fields in micelles of different sizes: (left ordinate) $\rho_{\mathrm{O}}(r)$, dashed lines; $\rho_{\mathrm{Na^+}}(r)$, circles; (right ordinate) $\rho_{\mathrm{SO_3^-}}(r)$, solid lines.

III. RESULTS

We begin with a brief discussion of the main structural features that are relevant for the characterization of solvation in reverse aqueous micelles. The micellar water pool is a nonuniform environment for electron solvation, so it is convenient to define a local coordinate system whose origin is at the center of the micelle. Letting r denote the magnitude of the distance from the center, the local density of species α, $\rho_\alpha(r)$, exhibits well-differentiated characteristics which depend on the species and size of the micelle. Except for the smallest micelles $(w_0<3)$, the water density in the central portion of the micelle is nearly uniform; for example, monitoring the oxygen atom in water one has $\rho_{\mathrm{O}}(r)\approx\rho_{\mathrm{O}}^{\mathrm{bulk}}=0.033\,\mathrm{Å}^{-3}$ (see Fig. 1).

This central region is the *bulk* or free water domain. Figure 1 also shows that $\rho_{\mathrm{O}}(r)$ has a deep minimum at $r\approx(R-4)$ Å. This minimum is flanked by two peaks at $r\approx(R-6.5)$ Å and $r\approx(R-2.5)$ Å where the water density shows considerable structure. The water in these region is termed *bound* and *trapped*, respectively.[9] The position of the peak at $r\approx(R-2.5)$ Å roughly coincides with the maximum in the local density of $\mathrm{Na^+}$, $\rho_{\mathrm{Na^+}}(r)$, which decays strongly for $r<(R-5)$ Å. The headgroup densities have sharp Gaussian profiles centered at $(R-2.5)$ Å in all cases.

A. Electron solvation

A reverse micelle is a complex environment for electron solvation. The central water pool can provide a medium which is favorable for solvation of the electron; however, if the electron explores regions of the micellar boundary it will encounter a very different environment, rich in counter ions and head groups, where its solvation structure is expected to be very different. Furthermore, counter ions are free to penetrate into the water pool and thus may form ion pair complexes with the electron.

In this work we focus on electron solvation in the central (bulk water) part of the micelle. As mentioned above, sudies of electron solvation in this central water pool must account for the fact that the electron may exist as an individual entity solvated by water, as a solvated ion pair species in combination with an $\mathrm{Na^+}$ counter ion or, possibly, as more complex ion-bound species. We limit our study to the solvation structure of a single electron and an electron–ion pair species. We shall see that electron–ion pair is the more stable species and is likely to play the most important role in determining the properties of the solvated electron in the micelle.

The structure of an individual electron in the central water pool, in the absence of electron–ion pairs, may be probed in several ways. The electron may be inserted at the micelle center and allowed to freely explore its environment. Due to the fact that the electron is preferentially solvated in certain regions in the micelle, a long trajectory starting from such initial conditions will mainly probe configurations in the vicinity of these favorable regions. Alternatively, the electron centroid $\mathbf{r}_C$,

$$\mathbf{r}_C=\frac{1}{\beta\hbar}\int_0^{\beta\hbar}\mathbf{r}(t)\,dt=\frac{1}{P}\sum_{i=1}^{P}\mathbf{r}_i \tag{5}$$

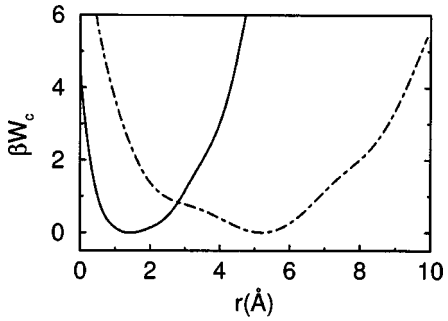

FIG. 2. Free energy as a function of the position of the electron centroid for different micelle sizes: $w_0=3$ (solid line); $w_0=7.5$ (dot–dashed line). The zeros of the mean potentials were arbitrarily set at the curve minima.

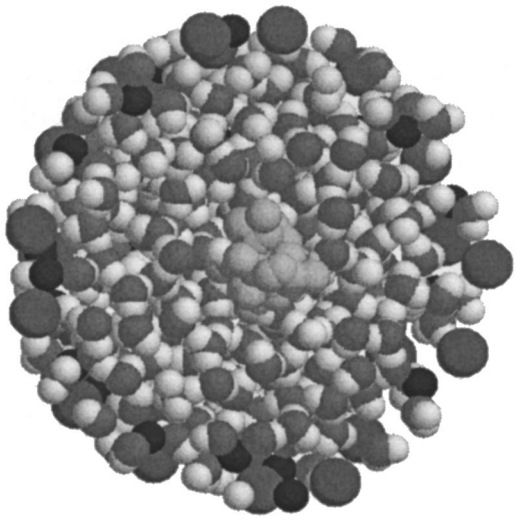

FIG. 3. Cross section of the micelle showing a molecular configuration of the internal structure of a $w_0=7.5$ aqueous reverse micelle with the electron–polymer (light gray) solvated in the central (bulk water) part of the aggregate. The counter ions and surfactant heads groups at the micelle boundary are rendered in black and dark gray shading, respectively.

may be fixed at a given distance from the micelle center by a holonomic constraint and the thermodynamic properties may be investigated using this constrained ensemble. Since the probability density of finding the electron centroid at a distance r from the center of the micelle is $P(r_C=r)=4\pi r^2\rho_C(r)$, where $\rho_C(r)$ is the local density of the electron centroid, the reversible work (difference in the potential of mean force) to move $\mathbf{r}_C$ along the radial direction from r' to r in the micelle is given by

$$W_C(r)-W_C(r')=-\frac{1}{\beta}\ln\frac{P(r_C=r)}{P(r_C=r')}, \\ =-\frac{1}{\beta}\ln\frac{\rho_C(r)}{\rho_C(r')}-\frac{2}{\beta}\ln\frac{r}{r'}. \tag{6}$$

The mean force $F_C(r)$ acting on the electron centroid is defined as

$$F_C(r)=-\frac{dW_C(r)}{dr}, \\ =-\langle\hat{\mathbf{r}}_C\cdot\boldsymbol{\nabla}_{\mathbf{r}_C}V_{\mathrm{eff}}\rangle_{r_C=r}+\frac{2}{\beta r}, \tag{7} \\ =-\sum_{i=1}^{P}\left\langle\hat{\mathbf{r}}_C\cdot\frac{dV_{\mathrm{eff}}}{d\mathbf{r}_i}\right\rangle_{r_C=r}+\frac{2}{\beta r},$$

where $\hat{\mathbf{r}}_C=\mathbf{r}_C/|\mathbf{r}_C|$ and the angle brackets $\langle\cdots\rangle_{r_C=r}$ represent a statistical average over an ensemble in which the electron centroid is constrained at $r_C=r$. The factor $2/(\beta r)$ in this equation, which has its origin in the spherical shell volume element, is an apparent force that can be viewed as arising from the noninertial nature of the radial centroid coordinate.[25]

Results for $W_C(r)$ for two micelle sizes are presented in Fig. 2. One can see that the most favorable radial positions for electron solvation in the $w_0=3$ and $w_0=7.5$ micelles correspond to $r_C\approx1.5$ and ≈5.25 Å, respectively. A rough estimate of the actual radial domain within which the electron centroid is likely to be found can be obtained by considering regions where $W_C(r)$ remains comparable to normal thermal energies. For $w_0=3.5$ this region is a spherical shell defined by $0.5\lesssim r\lesssim3$ Å, while for $w_0=7.5$ the corresponding shell is shifted and is defined by $2.5\lesssim r\lesssim7$ Å. Figure 3 shows a molecular configuration for the $w_0=7.5$ micelle with a solvated electron–polymer in the interior of the aqueous pool.

The decomposition of the total mean force into contributions from the solvent, Na^+ counter ions, and head groups shows that the average value of the force is the result of the balance between the force arising from the ionic field that tends to move the electron toward the micelle boundary and that from the water reactive field that tends to move the electron into the water pool. Thus, the sharp increase in W_C for large r should be interpreted as a stabilization of the electron in the central region induced by aqueous solvation.

The presence of an excess electron induces nonnegligible changes in the intramicelle spatial distributions of the different species. As expected, these effects are more noticeable in smaller micelles. In Fig. 4 we give results for $\rho_\alpha(r)$, α=O, Na^+. Comparison of these radial distributions with those for micelles without the electron is instructive. For $w_0=3$, in micelles containing an excess electron, the central part of the micelle is depleted of solvent due to the presence of the electron and has a more pronounced solvation structure. For larger aggregates, effects of the disruption of the solvent structure in the vicinity of an off-centered electron cannot be fully captured by the $\rho_\alpha(r)$ profiles since they involve an orientational average over the positions of the solvent molecules. The intramicelle spatial correlation functions for the Na^+ counter ions, also displayed in Fig. 4, are similar to those in micelles without an electron. Electron–solvent pair correlation functions are also of interest. In Fig. 5 we show the results for different centroid–solvent correlation functions $g_{C\alpha}(r)$ defined as

$$g_{C\alpha}(r)=\frac{1}{4\pi r^2}\left\langle\sum_i\ \delta(|\mathbf{r}_C-\mathbf{R}_i^\alpha|-r)\right\rangle, \tag{8}$$

where $\mathbf{R}_i^\alpha$ denotes the coordinate of site α in the ith molecule. For comparison, we have also included results for an

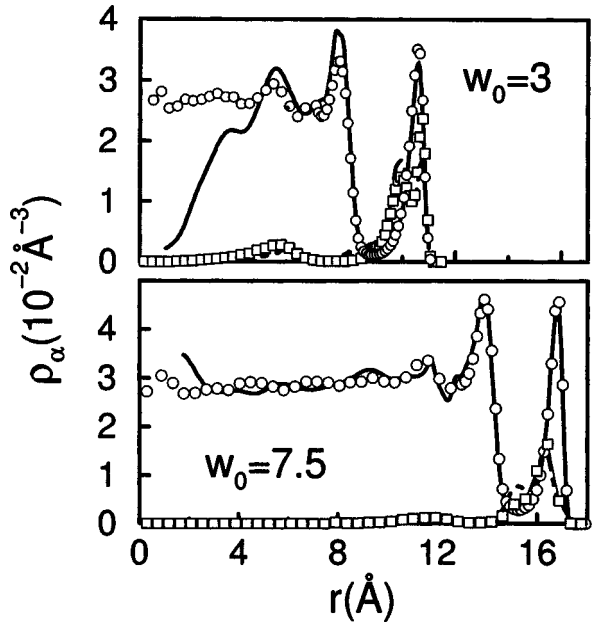

FIG. 4. Species density fields in micelles of different sizes in the presence of an excess electron solvated in the central region: $\rho_O(r)$ (solid lines), $\rho_{Na^+}(r)$ (dashed lines). The corresponding density profiles in absence of the excess electron are also shown (open circles and squares, respectively).

excess electron dissolved in bulk simple point charge (SPC) water. We see that in passing from the bulk to the smallest micelle, the spatial confinement in the micelle produces a gradual loss of solvent structure in the vicinity of the electron. However, the positions of the first solvation shells at $r \approx 3.5$ Å for $g_{CO}(r)$ and at $r \approx 2.45$ Å for $g_{CH}(r)$ are approximately the same, regardless of the micelle size, and are slightly shifted to larger distances compared to the bulk value. For $w_0 = 3$, only a well-defined first solvation shell containing five water molecules is observed; the boundaries of the second shell are affected by finite-size effects arising from the nearby interface. For larger aggregates, the first and second solvation shells are more easily distinguished. The

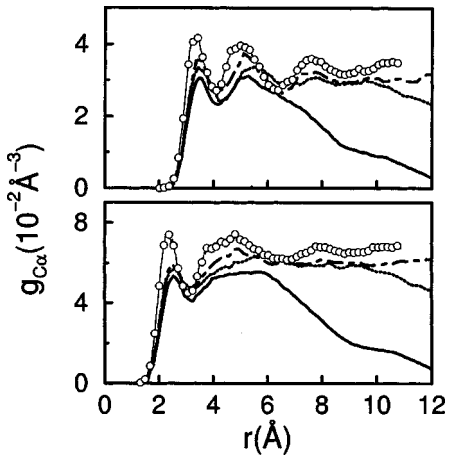

FIG. 5. Electron centroid–water pair correlation functions for different micelle sizes: (top panel) $g_{CO}(r)$; (bottom panel) $g_{CH}(r)$. Labels are $w_0 = 3$: solid lines; $w_0 = 7.5$: dotted lines; $w_0 = 10$: dot–dashed lines. Also shown results for an electron dissolved in bulk SPC water at ambient conditions (open circles).

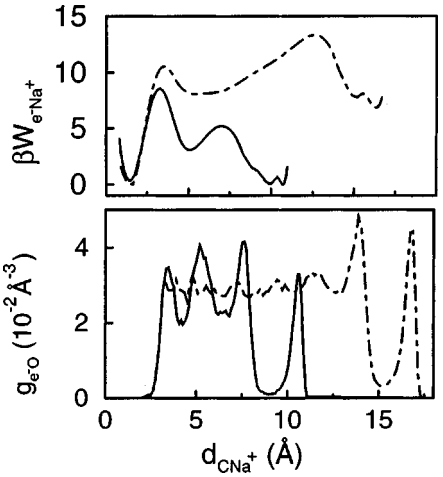

FIG. 6. Top panel: $e^- - Na^+$ potential of mean force for $w_0 = 3.5$ (solid line) and $w_0 = 7.5$ (dot–dashed line): (bottom panel) $e^- - O$ radial distribution functions (same labeling as the top panel). The results were obtained with the electron centroid constrained at $r = 0$.

integral over the first peak of g_{CO} shows that there are $n_O \approx 5.5$ and 5.7 molecules for sizes $w_0 = 7.5$ and 10, respectively, in the first solvation shell. These numbers are lower than the corresponding bulk value $n_O^{bulk} = 6$, where a single H atom in each water molecule is bound to the electron.

B. e^-–Na^+ ion pairs

We saw that excess electrons initially located at the micelle center are stabilized by aqueous solvation in the central water pool. These results were obtained from simulations with initial conditions where Na^+ counter ions were not present in the central water pool, and in the course of the simulations they rarely entered this water pool. These results should therefore be interpreted as a study of the metastable solvated electron far removed from any counter ions in the micelle.

However, it is important to consider the formation of $e^- - Na^+$ ion pairs within the micelle. The most direct way to study such ion pairs is by computing the electron–Na^+ mean potential W_{e-Na^+}. Given the nonuniformity of the system, and in order to facilitate comparisons between different micellar sizes, it is convenient to compute the mean potential with the electron centroid constrained at the micelle center. A full study would entail varying the electron centroid position as well as the centroid–counter ion distance but this is a very lengthy set of calculations for this inhomogeneous medium. In the top panel of Fig. 6 we present results for W_{e-Na^+} for $w_0 = 3$ and 7.5. The mean potentials were computed by integrating the average forces between the electron centroid and one tagged ion constrained to lie at ten fixed distances d_{C-Na^+} from the electron centroid. Both curves exhibit three minima. Stable configurations correspond to $e^- - Na^+$ contact ion pairs (CIPs) at $d_{C-Na^+} = 2$ Å. In addition, we also found stable solvent-separated-electron-ion pair (SSEIP) states characterized by $d_{C-Na^+} = 5.2$ Å. A third minimum corresponding to free ion (FI) states also appears in the vicinity of the micelle boundary $d_{C-Na^+} \approx (R - 2.5)$ Å. (This latter state corresponds to one of the solvation states studied in the

previous subsection.) The relative stabilities of these states depend on the micellar size; while in $w_0=3$ micelles the SSIP lies $2.5k_BT$ above the isoenergetic CIP and FI states, in larger aggregates the boundary FI state lies at nearly the same energy as the SSEIP state, and approximately $8k_BT$ above the CIP global minimum. The magnitudes of the CIP→SSEIP and SSEIP←FI interconversion free energy barriers are intermediate between $\Delta W \approx 5k_BT$ and $10k_BT$ and are high enough to prevent frequent transitions between different minima. A crude estimate of the characteristic time for such transitions $\tau_{\rm int}$ can be obtained from transition state theory, $\tau_{\rm int}^{\rm TST}=(2\pi/\omega_0)\exp(\beta\Delta W)\approx 0.1-10$ ns, where $\omega_0 \approx 10\,{\rm ps}^{-1}$ is a frequency characteristic of the free energy well minimum. In the course of very long simulation runs for unconstrained electrons, we did observe a few episodes of the spontaneous formation of CIP states in systems initially prepared in FI states. These rare trajectories were excluded from the ensemble used to obtain the results in Sec. III A.

Interestingly, also note that the positions of the free energy barriers roughly coincide with two well structured solvent shells within the micelle (see bottom panel of Fig. 6); one corresponding to the first solvation shell in the close vicinity of the electron and a second one identified with *bound* water, where both $g_{\rm CO}$ reach their global maxima. The presence of an intermediate shell with considerable structure at $r\approx 5.2$ Å in the $w_0=3$ case—which is clearly absent for $w_0=7.5$ micelles—also explains the deeper minimum corresponding to the SSEIP state in the smallest aggregates.

C. Electron localization

The last aspect that we consider concerns the extent of electron localization within the micelles. This localization may be probed by studying the behavior of $\mathcal{R}^2(t)$, the root mean square correlation function for the electron ''polymer chain'' defined by

$$\mathcal{R}^2(t-t')=\langle|\mathbf{r}(t)-\mathbf{r}(t')|^2\rangle, \quad 0\leqslant t-t'\leqslant\beta\hbar. \tag{9}$$

In bulk SPC water, under similar conditions, the temporal dependence of $\mathcal{R}(t)$ is characterized by a plateau value of approximately 3.1 Å which exists for all times with the exception of two short domains in the vicinity of $t=0$ and $t=\beta\hbar$. Such time independence has been interpreted as a signature of statistical dominance of the ground state on the behavior of the electron.[26] Expressed in terms of the spectrum of instantaneous electron eigenvalues, this situation corresponds to large energy gaps ($\gg k_BT$) between the ground state and the manifold of excited states. In Fig. 7 we present results for $\mathcal{R}(t)$ for three different micelle sizes.

We observe that as the electron polymer correlation length $\mathcal{R}=\mathcal{R}(\beta\hbar/2)$ decreases we move from smaller to larger aggregates. This trend is indicative of a gradual, more efficient electronic solvation; i.e., a larger extent of charge localization as we pass from small-size micelles to larger ones, with the $R\to\infty$ bulk result as the limiting value. Moreover, the increase in the electron size reveals that the overall external field generated by the counter ions and the surfactant head groups modifies the solvation characteristics of the central water core in a non-negligible way. Of course, the effects of the external field should be less important as the size of the micelle becomes much larger than the electron polymer size.

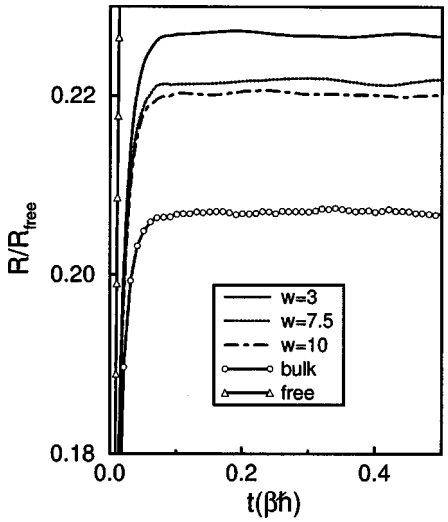

FIG. 7. Root mean square displacement for the electron polymer in different micelles. Also shown are results for bulk SPC water and a free electron.

IV. CONCLUSION

Solvated electrons are often used as probes of the structure of the interior of reverse micelles[3–7] and, consequently, it is important to be able to determine the nature of electron solvation in these small systems. Our microscopic investigations of the electron solvation structure have provided insight into some aspects of the solvation structure that are probed in such studies. The solvation of electrons in aqueous reverse micelles presents a number of distinctive features. As might be expected on physical grounds, we have found that the electron is preferentially solvated in the ''bulk'' water pool in the interior of the micelle, rather than in the ''surface'' water layer that is tightly bound to the surfactant head groups. However, for small micelles with $w_0\approx 3$ the presence of the electron strongly disturbs the equilibrium structure of the bulk water pool. In addition, the formation of electron–counter ion pairs plays a very important role in the electron solvation structure. For the two micelle sizes investigated, the most stable solvation state was the e^-–Na^+ CIP, but additional stable minima corresponding to SSEIP and FI states exist. Thus, our results indicate that the solvated electron should exist in an equilibrium population of these states determined by the free energy profile.

The formation of ion pairs can have important consequences for the spectral properties of solvated electrons in reverse micelles. In particular the observed blueshifts in the electron absorption peaks in reverse micelles relative to results for bulk water[3] appear to clash with the existence of a less favorably solvated and more delocalized electron. Consequently, it is important to assess the importance of contributions from e^-–Na^+ ion pairs to the total absorption spectrum, given the noticeable changes in the optical spectra of excess electrons dissolved in concentrated aqueous

electrolytes.[27] The quantum character of the electron is manifested in the decrease in the dispersion of the electron density with an increase in micelle size, reflecting a higher degree of solvation in the larger ''bulk'' water pools of the larger micelles.

We have focused solely on the equilibrium solvation structure but the dynamical properties of the solvated electron are also of interest. In particular the rate of exchange between the ''bulk'' and ''surface'' water pools depends on diffusion rates in the inhomogeneous micellar medium. The rates of exchange between contact, solvent-separated and free electron–counter ion pairs may be studied using rare event sampling methods to compute the rate constants for these processes. Computations of these dynamical properties present challenges since methods that combine quantum and classical dynamics at adiabatic and nonadiabatic levels of description must be used to obtain the results. Such dynamical studies along with investigations of the spectroscopic properties will help provide a more complete picture of electron solvation in aqueous reverse micelles.

ACKNOWLEDGMENTS

This work was supported in part by a grant from the Natural Sciences and Engineering Research Council of Canada. Partial financial support from Fundación Antorchas of Argentina is very much appreciated. D.L. is a staff member of CONICET (Argentina).

[1] For a series of articles on chemical reactivity in reverse micelles, see *Reverse Micelles*, edited by P. L. Luisi and B. E. Straub (Plenum, New York, 1984); and *Structure and Reactivity in Reverse Micelles*, edited by M. P. Pileni (Elsevier, Amsterdam, 1989).
[2] M. P. Pelini, J. Phys. Chem. **97**, 6961 (1993).
[3] M. Wong, M. Grätzel, and J. K. Thomas, Chem. Phys. Lett. **30**, 329 (1975).
[4] V. Calvo-Perez, G. S. Beddard, and J. H. Fendler, J. Phys. Chem. **85**, 2316 (1981).
[5] M. P. Pileni, B. Hickel, C. Ferrandini, and J. Pucheault, Chem. Phys. Lett. **92**, 308 (1982).
[6] M. P. Pileni, P. Brochette, B. Hickel, and B. Lerebours, J. Colloid Interface Sci. **98**, 549 (1984).
[7] J. L. Gebicki, L. Gebicka, and J. Kroh, J. Chem. Soc., Faraday Trans. **90**, 3411 (1994).
[8] B. Derecskei, A. Derecskei-Kovacs, and Z. A. Schelly, Langmuir **15**, 1981 (1999).
[9] J. Faeder and B. Ladanyi, J. Phys. Chem. B **104**, 1033 (2000); **105**, 11148 (2001).
[10] M. Sprik, R. W. Impey, and M. Klein, Phys. Rev. Lett. **56**, 2326 (1986); J. Stat. Phys. **43**, 949 (1986).
[11] J. Schnitker and P. J. Rossky, J. Chem. Phys. **86**, 3462 (1987).
[12] J. Schnitker and P. J. Rossky, J. Chem. Phys. **86**, 3471 (1987); B. J. Schwartz and P. J. Rossky, *ibid.* **101**, 6902 (1994), and references therein.
[13] A. Wallqvist, D. Thirumalai, and B. J. Berne, J. Chem. Phys. **86**, 6404 (1987).
[14] R. P. Feynman, *Statistical Mechanics* (Addison-Wesley, Reading, MA, 1972).
[15] M. E. Tuckerman, B. J. Berne, G. J. Martyna, and M. L. Klein, J. Chem. Phys. **99**, 2796 (1993).
[16] G. J. Martyna, M. E. Tuckerman, D. J. Tobias, and M. L. Klein, Mol. Phys. **87**, 1117 (1996).
[17] M. E. Tuckerman and A. Hughes, in *Classical and Quantum Dynamics in Condensed Phase Simulations*, edited by B. J. Berne, G. Ciccotti, and D. F. Coker (World Scientific, Singapore, 1998), Chap. 14.
[18] G. B. Bachelet, D. R. Hamann, and M. Schlüter, Phys. Rev. B **26**, 4199 (1982).
[19] H. J. C. Berendsen, J. P. M. Postma, W. F. Van Gunsteren, and J. Hermans, in *Intermolecular Forces*, edited by B. Pullman (Reidel, Dordrecht, 1981).
[20] H. J. C. Berendsen, J. R. Grigera, and T. P. Straatsma, J. Phys. Chem. **91**, 6269 (1987).
[21] D. Chandler and P. G. Wolynes, J. Chem. Phys. **74**, 4078 (1981).
[22] M. Tuckerman, B. J. Berne, and G. J. Martyna, J. Chem. Phys. **97**, 1990 (1992).
[23] S. Nosé, Mol. Phys. **52**, 255 (1984); W. G. Hoover, Phys. Rev. A **31**, 1695 (1985).
[24] J. P. Ryckaert, G. Ciccotti, and H. J. C. Berendsen, J. Comput. Phys. **23**, 327 (1977).
[25] E. A. Carter, G. Ciccotti, J. T. Hynes, and R. Kapral, Chem. Phys. Lett. **156**, 472 (1989).
[26] A. L. Nichols III, D. Chandler, Y. Singh, and D. Richardson, J. Chem. Phys. **81**, 5109 (1984).
[27] I. V. Kreitus, J. Phys. Chem. **89**, 1987 (1985).